*Journal of Applied Electrochemistry* **32**: 883–889, 2002.



# An electrochemical impedance study of hydrogen evolution and absorption on Sn-modified steel electrodes☆

L.F.P. DICK*, M.B. LISBOA[1] and E.B. CASTRO[2,*]
[1]*Departamento de Metalurgia, Universidade Federal do Rio Grande do Sul (UFRGS), Av. Osvaldo Aranha, 99, 6° andar, 90035-190, Porto Alegre, Brazil*
[2]*Instituto de Investigaciones Fisicoquímicas Teóricas y Aplicadas (INIFTA), Universidad Nacional de La Plata, Suc. 4 C.C. 16 (1900) La Plata, Argentina*
*(*authors for correspondence, e-mail: lfdick@vortex.ufrgs.br or bcastro@inifta.unlp.edu.ar)*

Received 22 June 2001; accepted in revised form 26 March 2002

*Key words:* hydrogen absorption, hydrogen embrittlement, hydrogen evolution reaction, impedance spectroscopy

**Abstract**

In this work we report results related to hydrogen evolution and absorption, on AISI 1045 steel and AISI 1045 steel modified by Sn electrodeposition, in 1 M NaOH. The simulation of experimental impedance, steady-state $j/E$ data and electrochemical permeation data in terms of the Volmer–Heyrovsky mechanism coupled to H absorption and diffusion, allowed the estimation of kinetic and transport parameters leading to an appropriate interpretation of diminished H absorption on Sn modified samples.

## 1. Introduction

The ingress of H into ferrous materials has been the subject of numerous investigations, due to it being a major cause of embrittlement and damage coupled to metallic corrosion in many technological processes. It is well known that H adatoms, $H_{ad}$, produced in the Volmer step by electrochemical reduction of $H_2O$ or $H_3O^+$, may subsequently penetrate and diffuse into the electrode material [1]. Consequently, this process may be hindered by modification of the hydrogen evolution reaction (HER) kinetics, in order to diminish the $H_{ad}$ surface concentration or by changing the kinetics of H absorption, or H solubility. It has been reported [2, 3] that Fe electrodes modified by Sn implantation and electrodeposition, exhibit diminished steady state H permeation rates compared to pure Fe, due to smaller H concentrations in the electrode material.

In this work, we report results related to hydrogen evolution and absorption on AISI 1045 steel electrodes, modified by Sn electrodeposition and annealing. The simulation of experimental impedance and electrochemical permeation data in terms of Volmer–Heyrovsky reaction steps coupled to H absorption and diffusion [4], allowed the estimation of kinetic and transport parameters leading to an appropriate interpretation of the diminished H absorption on Sn-modified samples.

## 2. Experimental details

The Sn modified electrodes were prepared by electrodeposition of a 100 nm thick Sn layer, from a solution containing $SnSO_4$ 30 g $l^{-1}$, $H_2SO_4$ 100 ml $l^{-1}$ and a commercial brightener (ROHCO roplate), on AISI 1045 steel samples inserted in epoxy resin (exposed geometric area, $A_g = 1$ cm$^2$). To promote Sn diffusion and formation of Fe–Sn compounds, the samples were annealed for 2 h at 400 °C in low vacuum ($10^{-2}$ atm).

Electrochemical experiments were carried out in 0.1 M NaOH solutions, at $T = 25$ °C, in a conventional three-compartment glass cell [4], under $N_2$ atmosphere. Potentials were measured and referred to in the text, against a Hg/HgO/0.1 M $OH^-$ reference electrode.

Potentiostatic polarization curves were measured with an EG&G M273 potentiostat. Impedance spectra were recorded, using a Solartron 1255HF FRA and PAR 273 potentiostat coupled to an IBM compatible PC.

## 3. Results

Figure 1 shows polarization plots corresponding to HER on Sn-modified steel (Sn–St) and on untreated steel electrodes (St). Experimental potential values were

☆ This paper was initially presented at the 5th International Symposium on Electrochemical Impedance Spectroscopy at Marilleva, Trento, Italy, June 2001.

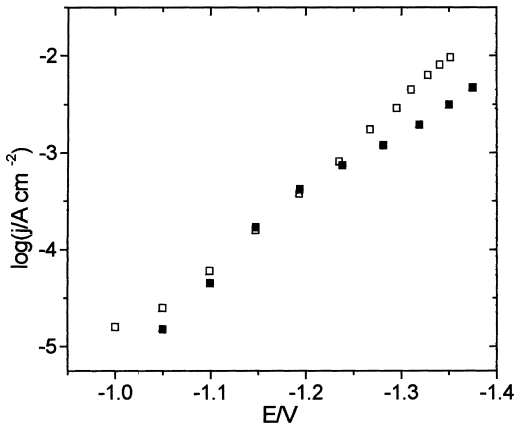


*Fig. 1.* Polarization plots for HER in 0.1 M NaOH on untreated steel and on Sn-modified steel electrodes. Key: (□) Sn–St; (■) steel.

corrected for ohmic drop effects with electrolyte resistance ($R_s$) values obtained from impedance measurements. Current densities, $j$, were calculated per unit of geometric area, $A_g$.

Sn-modified steel electrodes show a Tafel slope of $b_T \approx 0.12$ V dec$^{-1}$ in the whole measured potential range, while for untreated steel electrodes a value of $b_T \approx 0.18$ V dec$^{-1}$ was calculated at high HER current densities, $j > 0.5$ mA cm$^{-2}$. At potentials $|E| > 1.25$ V, higher current densities were measured on Sn-modified steel compared to untreated steel electrodes.

The linearity of Tafel plots, with $0.180 \text{ V dec}^{-1} \geqslant b_T \geqslant 0.120 \text{ V dec}^{-1}$, at high negative overpotentials, is a strong indication that the HER proceeds via a Volmer–Heyrovsky mechanism [5]. It has been reported [1, 6] that the Volmer–Heyrovsky scheme rules the HER on Fe and steel in alkaline and neutral electrolytes.

In the case of the Volmer–Tafel mechanism an activation controlled limiting current arises at high cathodic overpotentials [7], this behaviour has been reported for very few metal surfaces.

Figures 2 and 3 depict complex impedance spectra of St and Sn–St electrodes, corresponding to different potentials in the HER region. In both cases distorted capacitive contributions are observed in impedance spectra at low HER overpotentials (Figures 2(a, b) and 3(a, b)). At higher cathodic overpotentials two overlapped capacitive loops may be distinguished (Figure 2(d)).

Double layer capacitance values, $C_{dl}$, calculated from high frequency data indicate interfacial areas ten times bigger for Sn–steel electrodes as compared to pure steel (Table 1). The enhancement of the interfacial area could be explained by the reduction under cathodic polarization of superficial Fe–Sn oxides, which were formed previously during the annealing. The analysis by Rutherford backscattering spectroscopy [3] of the surface indicated the presence after annealing of a 10 nm thick oxide layer. Thus, the described increment of interfacial area was assumed to be due to the formation of Fe–Sn dendrites by the reduction of surface oxides.

### 3.1. *Reaction mechanism*

The experimental data presented in Figures 1–3 may be analysed according to the following reaction steps [4, 8]:

*Volmer*

$$H_2O + M + e^- \underset{K_{-1}}{\overset{K_1}{\rightleftharpoons}} MH_{ad} + OH^- \qquad \text{(I)}$$

*Heyrovsky*

$$MH_{ad} + H_2O + e^- \underset{K_{-2}}{\overset{K_2}{\rightleftharpoons}} M + H_2 + OH^- \qquad \text{(II)}$$

*Tafel*

$$MH_{ad} + MH_{ad} \underset{K_{-3}}{\overset{K_3}{\rightleftharpoons}} 2\,M + H_2 \qquad \text{(III)}$$

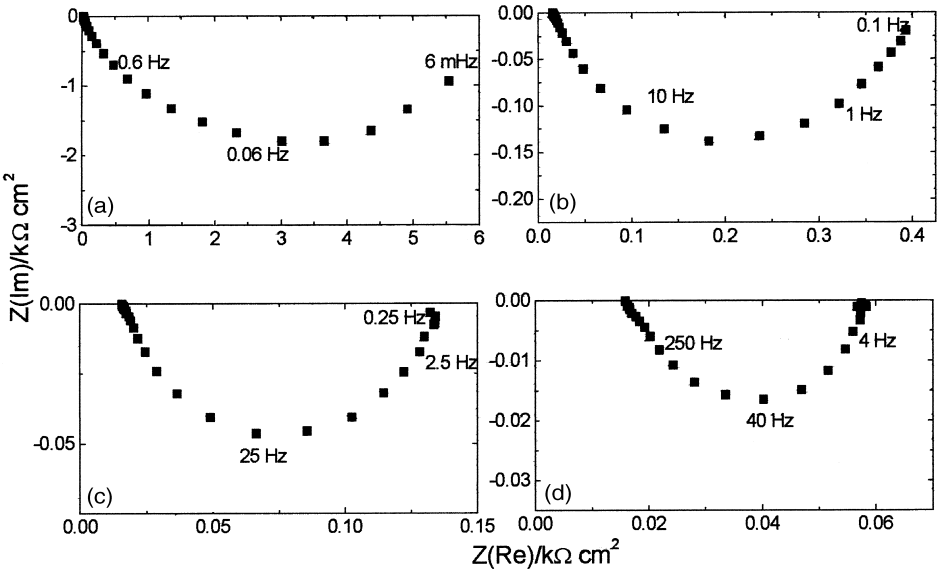


*Fig. 2.* Complex impedance spectra corresponding to HER on untreated steel. $E_{app}$: (a) −1.05, (b) −1.15, (c) −1.25 and (d) −1.35 V.

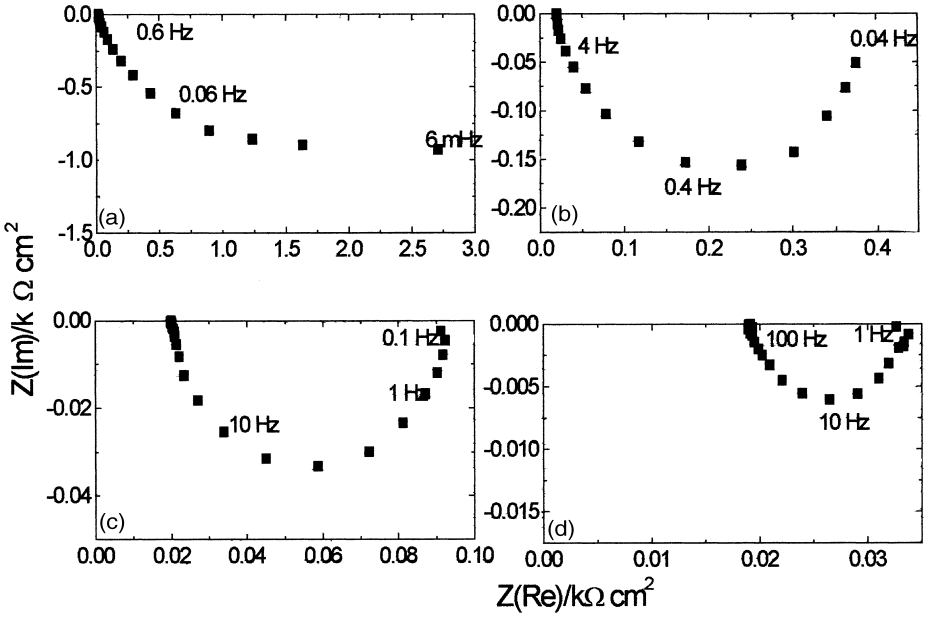


*Fig. 3.* Complex impedance spectra corresponding to HER on Sn-modified steel. $E_{app}$: (a) −1.05, (b) −1.15, (c) −1.25 and (d) −1.35 V.

*Table 1.* Parameters used for the simulation of impedance and steady-state $i/E$ data
Constraints $b_i$–$b_{-i}$ = −38.9 $V^{-1}$ and $K_1^{eq}K_2^{eq}/K_{-1}^{eq}K_{-2}^{eq} = 1$, were applied
Real area, $A_r$, was estimated from $C_{dl}$ values calculated from high frequency impedance data

| | $A_r$ /cm$^{-2}$ | $K_1^0/A_r$ /mol s$^{-1}$ cm$^{-2}$ | $b_1$ /V$^{-1}$ | $K_2^0/A_r$ /mol s$^{-1}$ cm$^{-2}$ | $b_2$ /V$^{-1}$ | $K_{-1}^0/A_r$ /mol s$^{-1}$ cm$^{-2}$ | $K_4$ /$K_{-4}$ | $DC_{H,max}$ /mol cm$^{-1}$ s$^{-1}$ | $\Gamma/A_r$ /mol cm$^{-2}$ | $C_{dl}/A_r$ /F cm$^{-2}$ |
|---|---|---|---|---|---|---|---|---|---|---|
| Steel | 1 | $(6 \pm 1) \times 10^{-21}$ | −23.4 | $(6 \pm 0.5) \times 10^{-16}$ | −12.6 | $(3 \pm 1) \times 10^{-2}$ | $1.2 \pm 0.4$ | $3.5 \times 10^{-12}$ | $6 \times 10^{-10}$ | $1 \times 10^{-4}$ |
| Sn–St | 10 | $(2 \pm 0.4) \times 10^{-19}$ | −19.9 | $(2 \pm 0.05) \times 10^{-20}$ | −19.2 | $(4 \pm 0.7) \times 10^{-1}$ | 0.03 | $\leqslant 3.5 \times 10^{-12}$ | $4 \times 10^{-10}$ | $1.4 \times 10^{-4}$ |

In the following analysis $v(III) << v(II)$ will be considered, according to the Tafel behaviour depicted in Figure 1. This assumption will be validated by the parametric identification presented below.

H atoms may be absorbed into the electrode material according to the following reaction [9]:

*H absorption reaction (HAR)*

$$MH_{ad} \underset{K_{-4}}{\overset{K_4}{\rightleftharpoons}} M + H_{ab} \qquad \text{(IV)}$$

Reaction IV is followed by H diffusion into the bulk of the metal. In the steady state, equilibrium of Reaction IV is usually assumed [7, 8].

Equations relating charge and mass balances are given by the following $I_F(t)$ and $g(t)$ functions [8]:

$$I_F(t) = -F[K_1(1-\theta) - K_{-1}\theta + K_2\theta - K_{-2}(1-\theta)] \qquad (1)$$

$$\begin{aligned} g(t) &= \Gamma \frac{d\theta}{dt} \\ &= K_1(1-\theta) - K_{-1}\theta - K_2\theta + K_{-2}(1-\theta) \\ &\quad - K_4\theta(1-X_H) + K_{-4}(1-\theta)X_H \end{aligned} \qquad (2)$$

where $K_i = K_i^0 \exp(b_i E)$, with $b_i = -\beta_i F/RT$, $b_{-i} = (1-\beta_i)F/RT$. Also: $E$, corresponding to the applied potential ($E_{app}$) corrected by ohmic drop effects, is given by $E = E_{app} - (IR_s)$; $K_4$, $K_{-4}$ being the absorption reaction (IV) chemical rate constants; $\theta$ is the $H_{ad}$ surface coverage and $\Gamma$ the $H_{ad}$ maximum surface concentration; and $X_H = C_H/C_{H,max}$, being $C_H$ the $H_{ab}$ concentration inside the metal (at $x = 0$, just below the surface), where $C_{H,max}$, is the maximum $H_{ab}$ interstitial concentration, also called the critical concentration, $C_{crit}$ [10].

At the equilibrium potential, the following condition operates [8]:

$$\frac{K_1^{eq}K_2^{eq}}{K_{-1}^{eq}K_{-2}^{eq}} = 1$$

eliminating one out of four kinetic constants.

Hydrogen transport into the metal is described by Fick's first and second laws [4, 8]. Semiinfinite diffusion along the $x$ direction will be considered on account of the geometry of the electrode:

$$J(x,t) = -DC_{H,max}\left[\frac{\partial X_H(x,t)}{\partial x}\right] \qquad (3)$$

$$\frac{dX_H(x,t)}{dt} = D\left[\frac{\partial^2 X_H(x,t)}{\partial x^2}\right] \qquad (4)$$

The boundary condition at $x = 0$, is given by

$$J(0,t) = v_{IV} = K_4\theta(1-X_H) - K_{-4}(1-\theta)X_H$$

Considering the steady-state conditions [7, 8]: the solution of Equation 4, for semiinfinite diffusion under steady state conditions, indicates $J(x) = 0$ [11]. Thus,

$$J(0) = v_{IV} = K_4\theta(1 - X_H) - K_{-4}(1 - \theta)X_H = 0$$

and equilibrium of Reaction IV is fulfilled under steady-state conditions.

Also, taking into account $d\theta/dt = 0$, the following steady state equations may be derived:

$$\theta^{SS} = \frac{K_1 + K_{-2}}{K_1 + K_{-1} + K_2 + K_{-2}} \tag{5}$$

$$X_H^{SS} = \frac{K_4\theta}{K_4\theta + K_{-4}(1 - \theta)} = \frac{\frac{K_4}{K_{-4}}\theta}{\frac{K_4}{K_{-4}}\theta + (1 - \theta)} \tag{6}$$

$I_F^{SS}$ may now be calculated using Equations 1 and 5.

### 3.2. *Faradaic impedance analysis*

The faradaic impedance, $Z_F$, for this system, may be derived from Equations 1–4 after a Taylor series expansion limited to the first order terms and a Fourier transformation, as explained in [4, 12].

$$\frac{1}{Z_f} = \frac{\Delta I_F(\omega)}{\Delta E(\omega)} = \left(\frac{\partial I_F}{\partial E}\right)_\theta + \left(\frac{\partial I_F}{\partial \theta}\right)_E \frac{\Delta\theta(\omega)}{\Delta E(\omega)} \tag{7}$$

$$\Gamma j\omega\frac{\Delta\theta(\omega)}{\Delta E(\omega)} = \left(\frac{\partial g}{\partial E}\right)_{\theta,C_H} + \left(\frac{\partial g}{\partial \theta}\right)_{E,C_H}\frac{\Delta\theta(\omega)}{\Delta E(\omega)} + \left(\frac{\partial g}{\partial X_H}\right)_{E,\theta}\frac{\Delta X_H(0,\omega)}{\Delta E(\omega)} \tag{8}$$

To determine $\Delta X_H(0,\omega)/\Delta E$, Equation 4 must be solved for a small sine-wave potential perturbation of the system. After Fourier transformation, Equation 4 may be written as

$$j\omega\Delta X_H(x,\omega) = D\left(\frac{\partial^2 \Delta X_H(x,\omega)}{\partial x^2}\right) \tag{9}$$

Following a similar procedure, Equation 3 may be expressed as

$$\Delta J(x,\omega) = -DC_{H,max}\left(\frac{\partial \Delta X_H(x,\omega)}{\partial x}\right) \tag{10}$$

Equation 9 has the solution:

$$\Delta X_H(x,\omega) = M\ \exp(x\sqrt{j\omega/D}) + N\ \exp(-x\sqrt{j\omega/D})$$

with the following boundary conditions:
At $x \to \infty$, for semiinfinite diffusion, $\Delta X_H(x,\omega) \to 0$. Thus,

$$\Delta X_H(x,\omega) = N\ \exp(-x\sqrt{j\omega/D}) \tag{11}$$

At $x = 0$,

$$A_g\Delta J(0,\omega) = \Delta v_{IV}(\omega) = -A_g DC_{H,max}\frac{\partial \Delta X_H(0,\omega)}{\partial x} \tag{12}$$

where $v_{IV}$ is the reaction rate of step IV.

Therefore, taking into account Equations 10–12:

$$\frac{\Delta v_{IV}(\omega)}{\Delta E(\omega)} = \left(\frac{\partial v_{IV}}{\partial \theta}\right)\frac{\Delta\theta(\omega)}{\Delta E(\omega)} + \left(\frac{\partial v_{IV}}{\partial X_H}\right)\frac{\Delta X_H(\omega)}{\Delta E(\omega)} = A_g DC_{H,max}\sqrt{\frac{jw}{D}}\frac{\Delta X_H(\omega)}{\Delta E(\omega)} \tag{13}$$

The set of equations (7, 8 and 13) may be rewritten as follows:

$$\frac{1}{Z_F} = -F[K_1b_1(1 - \theta^{ss}) - K_{-1}b_{-1}\theta^{ss} + K_2b_2\theta^{ss} - K_{-2}b_{-2}(1 - \theta^{ss})] + (-K_1 - K_{-1} + K_2 + K_{-2}) \times \frac{\Delta\theta(\omega)}{\Delta E(\omega)} \tag{14}$$

$$\Gamma j\omega\frac{\Delta\theta(\omega)}{\Delta E(\omega)} = [K_1b_1(1 - \theta^{ss}) - K_{-1}b_{-1}\theta^{ss} - K_2b_2\theta^{ss} + K_{-2}b_{-2}\theta^{ss}] + [-K_1 - K_{-2} - K_{-1} - K_2 - K_4(1 - X_H^{ss}) - K_{-4}X_H^{ss}]\frac{\Delta\theta(\omega)}{\Delta E(\omega)} + [K_4\theta^{ss} + K_{-4}(1 - \theta^{ss})]\frac{\Delta X_H(0,\omega)}{\Delta E(\omega)} \tag{15}$$

$$[K_4(1 - X_H^{ss}) + K_{-4}X_H^{ss}]\frac{\Delta\theta(\omega)}{\Delta E(\omega)} - [K_{-4}(1 - \theta^{ss}) + K_4\theta^{ss}]\frac{\Delta X_H(0,\omega)}{\Delta E(\omega)} = ArDC_{H,max}\sqrt{\frac{j\omega}{D}}\frac{\Delta X_H(0,\omega)}{\Delta E(\omega)} \tag{16}$$

The linear set of equations (Equations 14–16) may be written in matrix notation as [4]:

$$HA = Y \tag{17}$$

where

$$H = \begin{vmatrix} -1 & h_{1,2} & 0 \\ 0 & h_{2,2} & h_{2,3} \\ 0 & h_{3,2} & h_{3,3} \end{vmatrix}$$

$$h_{1,2} = -F(-K_1 + K_{-2} - K_{-1} + K_2)$$
$$h_{2,2} = (-K_1 - K_{-2} - K_{-1} - K_2 - K_4(1 - X_H^{ss}) - K_{-4}X_H^{ss} - \Gamma j\omega)$$
$$h_{2,3} = K_{-4}(1 - \theta^{ss}) + K_4\theta^{ss}$$
$$h_{3,2} = -(K_4(C_{H,max} - C_H^{ss}) + K_{-4}C_H^{ss})$$
$$h_{3,3} = A_g DC_{H,max}\sqrt{\frac{j\omega}{D}} + K_{-4}(1 - \theta^{ss}) + K_4\theta^{ss}$$

$$A = \begin{vmatrix} 1/Z_f \\ \Delta\theta(\omega)/\Delta E(\omega) \\ \Delta X_H(\omega)/\Delta E(\omega) \end{vmatrix}$$

and

$$Y = \begin{vmatrix} y_{1,1} \\ y_{2,1} \\ 0 \end{vmatrix}$$

with

$$y_{1,1} = F(K_1 b_1(1-\theta^{ss}) - K_{-1} b_{-1}\theta^{ss} + K_2 b_2 \theta^{ss} - K_{-2} b_{-2}(1-\theta^{ss}))$$

$$y_{2,1} = -(K_1 b_1(1-\theta^{ss}) - K_{-1} b_{-1}\theta^{ss} - K_2 b_2 \theta^{ss} + K_{-2} b_{-2}\theta^{ss})$$

The solution of Equation 17 is

$$A = H^{-1} Y \tag{18}$$

From Equation 18, $Z_F = (A_{1,1})^{-1}$ may be derived by giving numerical values to the parameters $D$, $K_i$, $b_i$, $\Gamma$ and $C_{H,max}$.

For the calculation of the total impedance function, $Z_T$, parallel connection of $Z_F$ with $C_{dl}$, and series connection of both with the electrolyte resistance, $R_S$, must be considered [4]:

$$Z_T = R_S + Z_F(1 + j\omega C_{dl} Z_F)^{-1} \tag{19}$$

### 3.3. *Simulation results*

Figure 4 shows experimental and simulated Nyquist plots corresponding to HER on steel and Sn-modified steel electrodes. Simulated data were calculated in terms of Equations 18 and 19, using the system parameter values in Table 1. Good agreement is also observed between experimental and theoretical steady state polarization data depicted in Figure 5.

Kinetic and permeation parameters, $K_4/K_{-4}$ and $DC_{Hmax}$ related to H absorption and diffusion on Sn–steel could not be determined with sufficient precision from impedance simulation, as the contribution of Reaction IV is smaller on Sn–steel electrodes than on untreated steel. Nevertheless impedance data corresponding to Sn–steel, could only be adequately simulated with values of $DC_{H,max} \leqslant 3.5\times10^{-12}$ mol cm$^{-1}$ s$^{-1}$.

According to $DC_{H,max}$ value given in Table 1, $C_{H,max} \approx 5 \times 10^{-8}$ mol cm$^{-3}$, was estimated for both materials, assuming $D \approx 7 \times 10^{-5}$ cm$^2$ s$^{-1}$ [1].

The $K_4/K_{-4}$ value corresponding to Sn–steel, in Table 1, was determined from electrochemical permeation data as explained below.

The potential dependence of the kinetic constants may be calculated in terms of $K_i$ and $b_i$ values assembled in Table 1. As depicted in Figure 6, Heyrovsky reaction corresponds to the rate determining step (r.d.s.), for both materials.

The $\theta^{ss}$ against $E$ dependence, corresponding to steel and Sn–steel is depicted in Figure 7.

For Sn–steel electrodes, it was not possible to determine $K_4/K_{-4}$, with acceptable precision, from impedance simulation. This parameter was determined, from Equation 6, using experimental $X_H^{ss}$ values determined by electrochemical permeation [2, 3], and $\theta^{ss}$, calculated from Equation 5. With this procedure $K_4/K_{-4} = 0.03$, was estimated as indicated in Table 1. Good simulation results of impedance data were obtained using this value for $K_4/K_{-4}$.

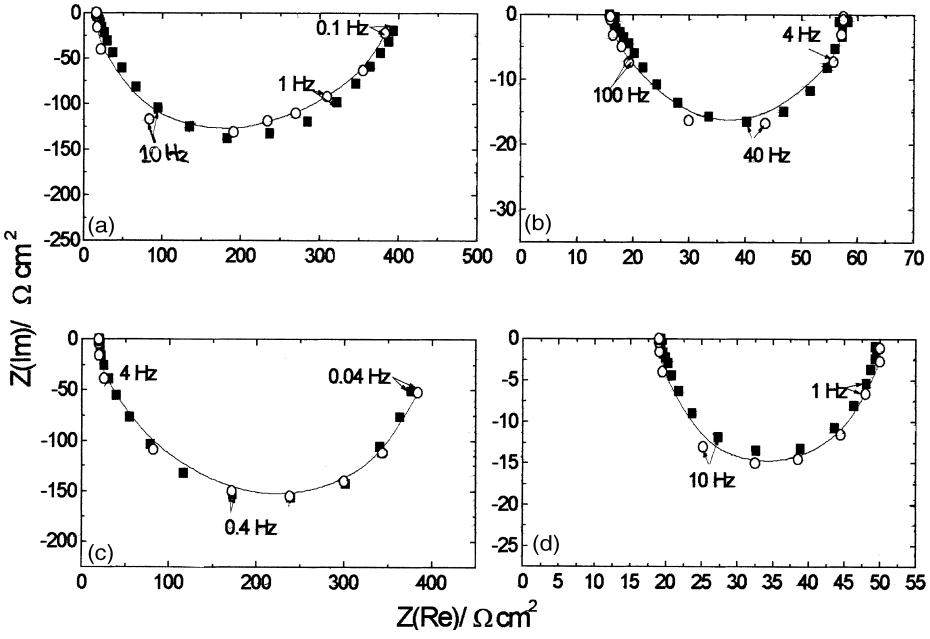


*Fig. 4.* Experimental and simulated complex impedance spectra, corresponding to steel and Sn-modified steel electrodes. $E_{app}$: (a) −1.15 V (steel); (b) −1.35 V (steel); (c) −1.15 V (Sn–steel); (d) −1.3 V (Sn–steel). Key: (■) experiment and (○) simulation.

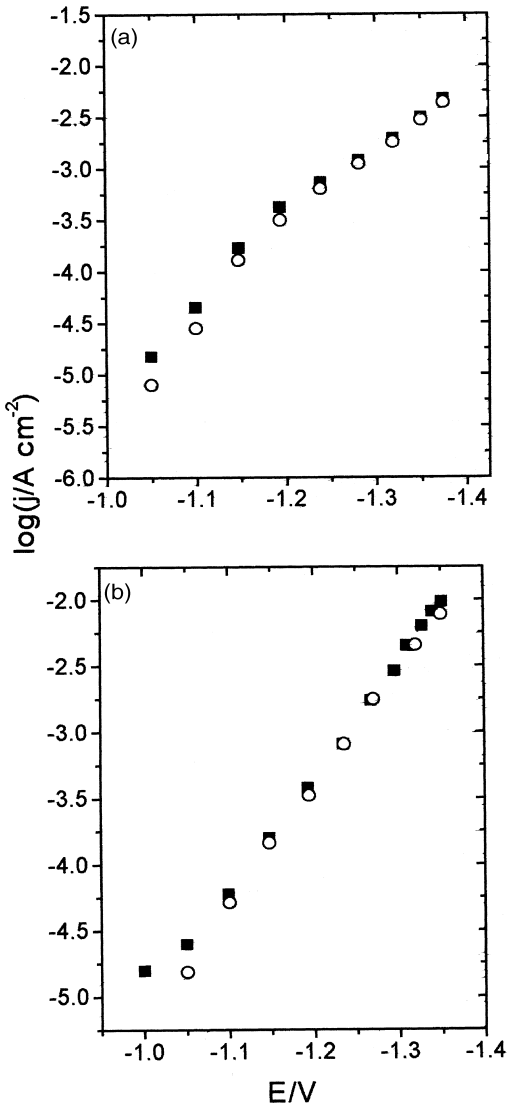


*Fig. 5.* Experimental and simulated $j/E$ data corresponding to HER on steel (a) and Sn–steel (b) electrodes. Key: (■) experiment and (○) simulation.

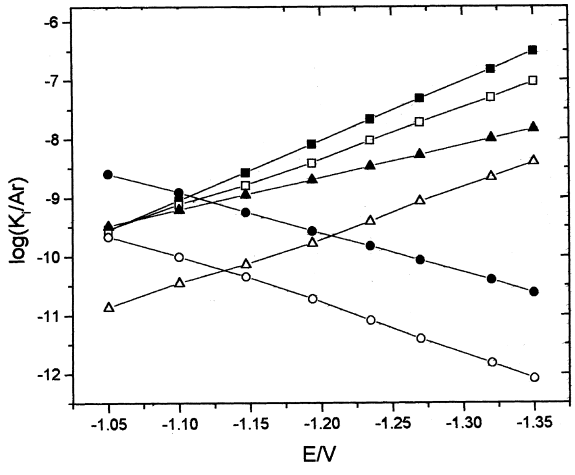


*Fig. 6.* $\log(K_i/A_r)$ against $E$ plots corresponding to Volmer and Heyrovsky reactions on St and Sn–St electrodes. Key: (■) $K_1$ (St); (□) $K_1$ (Sn–St); (●) $K_{-1}$ (St); (○) $K_{-1}$ (Sn–St); (▲) $K_2$ (St); (△) $K_2$ (Sn–St).

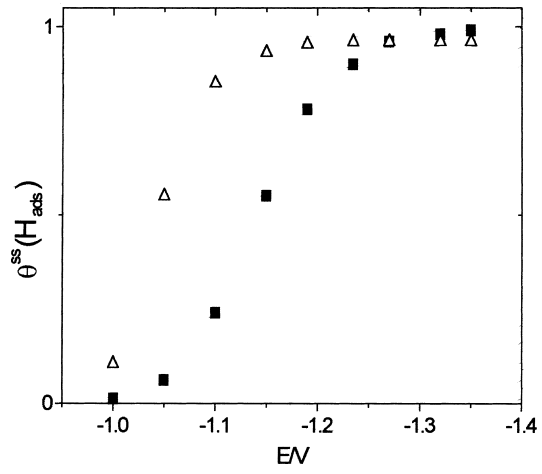


*Fig. 7.* Steady-state $\theta$ ($H_{ad}$) against $E$ plots, calculated with Equation 5 using the kinetic parameters of Table 1. Key: (■) steel and (△) Sn–steel.

$X^{ss}$ against $j$ plots for St and Sn–St are depicted in Figure 8. For steel, good agreement is observed between $X^{ss}$ in Figure 8 and reported electrochemical permeation results [1–3].

In Figure 7, $\theta^{ss}$ against $E$ plots, indicate higher values of $H_{ad}$ surface coverage, $\theta^{ss}$, for Sn-modified steel electrodes for $|E| < 1.25$ V. Nevertheless, electrochemical permeation data (Figure 8) indicate smaller $X_H^{ss}$ (and smaller $C_H^{ss}$, for the same $C_{H,max}$) for Sn-modified steel. Accordingly, smaller $X_H$ values in Sn–steel electrodes are a consequence of a lower $K_4/K_{-4}$ ratio, as indicated in Table 1.

In Figure 9, theoretical $X_H^{ss}$ against $(j)^{1/2}$ plots corresponding to steel and Sn–steel, are depicted. Clearly a linear dependence is observed for steel electrodes at low $j$. A linear dependence in, (permeation current) $I_p$ against $j^{1/2}$ plots has been taken as proof of Volmer–Tafel controlling mechanism [13].

$I_p$ is related to $X_H^{ss}$ through:

$$I_p = zFDA_gC_{H,max}X_H^{ss}/L$$

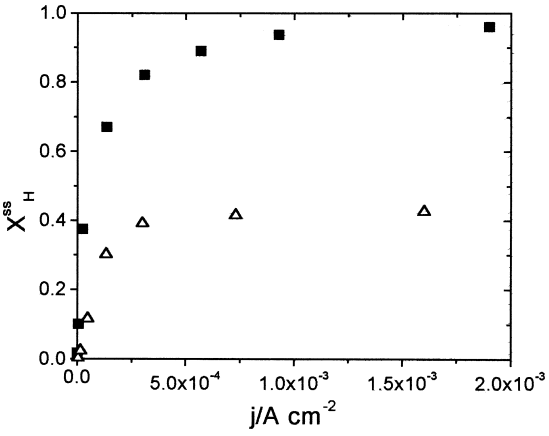


*Fig. 8.* $X_H^{ss}$ against $j$ plots. Key: (■) steel and (△) Sn–steel.

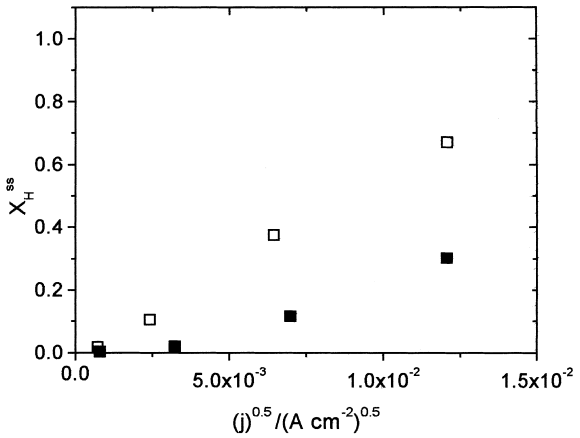


*Fig. 9.* Theoretical $X_H^{ss}$ against $j^{1/2}$ plots calculated with Equations 5 and 6. Key: (□) steel and (■) Sn–steel.

where $L$ is the metallic membrane thickness. Then, Figure 9 indicates that permeation data alone do not give conclusive evidence for the determination of the mechanism controlling the HER.

## 4. Conclusions

(i) Steady state $j/E$ and electrochemical impedance data corresponding to hydrogen evolution and absorption on steel and Sn modified steel electrodes in 1 M NaOH were adequately simulated in terms of the Volmer–Heyrovsky reaction scheme coupled to hydrogen absorption and diffusion.

(ii) Diminished hydrogen concentrations in Sn modified steel in comparison with steel electrodes, are due to a smaller $K_4/K_{-4}$, absorption/desorption reaction rates ratio.

## References

1. E.G. Dafft, K. Bohnenkamp and H.J. Engell, *Corros. Sci.* **19** (1979) 591.
2. M.V.F. Coelho and L.F.P. Dick, XIII SIBAE-Simpósio Ibero-americano de Eletroquímica, actas del congreso E21 (1998), santiago dechile (1998); electrochemical and solid state letters (submitted) (not available).
3. M.B. Lisboa and L.F.D. Dick, XII SIBEE-Simpósio Brasileiro de Eletroquímica e Eletroanalítica, C199 (2001) Tec art Editora Ltda, Gramado, Brasil (2001).
4. E.B. Castro, M.J. de Giz, E.R. Gonzalez and J.R. Vilche, *Electrochim. Acta* **42** (1997) 951.
5. A. Lasia and A. Rami, *J. Electroanal. Chem.* **294** (1990) 123.
6. R.F. Blundy and L.L. Shreier, *Corros. Sci.* **17** (1977) 509.
7. B.E. Conway and Jerkiewicz, *J. Electroanal. Chem.* **357** (1993) 47.
8. A. Lasia and D. Grégoire, *J. Electrochem. Soc.* **142** (1995) 3393.
9. J.O'M. Bockris, J. McBree and L. Nanis, *J. Electrochem. Soc.* **112** (1965) 1025.
10. J.O'M. Bockris and P.K. Subramanyan, *J. Electrochem. Soc.* **118** (1971) 1114.
11. J.L. Crank, 'The Mathematics of Diffusion' (Oxford University Press, Oxford (1964), pp. 18–25.
12. Ch. Lim and Su-il Pyun, *Electrochim. Acta* **38** (1993) 2645.
13. R.N. Iyer, H. Pickering and M. Zamanzadeh, *J. Electrochem. Soc.* **136** (1989) 2463.